

# Gamma-Ray Instrument for Polarimetry, Spectroscopy and Imaging (GIPSI)

R.A. Kroeger, W.N. Johnson, R.L. Kinzer, J.D. Kurfess  
Naval Research Laboratory  
Washington, DC 20375

S.E. Inderhees, B.F. Philips  
Universities Space Research Association  
Washington, DC

B.L. Graham  
George Mason University  
Fairfax, VA

## ABSTRACT

We present an instrument concept called GIPSI that uses germanium strip detectors in an imaging system to provide narrow line sensitivity  $< 8.0 \times 10^{-6} \gamma \text{ cm}^{-2} \text{ s}^{-1}$  at 100 keV in a 2 week exposure ( $3\sigma$ ), and which has a point spread function (spatial resolution) of approximately 20 arc minutes rms. The germanium strip detectors also make an excellent polarimeter by capitalizing on the angular dependence of the Compton scattering cross section. Gamma-ray polarimetry in the energy band around 60–300 keV is an interesting area of high energy astrophysics where observations have not been possible with the technologies employed in current and past space missions. We have tested a prototype detector with polarized beams and have measured a modulation factor of approximately 0.8 at 100 keV. A sensitive instrument can be realized on a modest space mission or a long duration balloon flight. Linear polarization can be detected in sources such as the Crab Pulsar, Cen A, Cyg X–1, and solar flares down to less than 5% of the source flux. The proposed instrument would have a collecting area of 400 cm<sup>2</sup>.

Keywords: Imaging, spectroscopy, polarimetry, gamma-rays

## 1 INTRODUCTION

The Gamma-Ray Instrument for Polarimetry, Spectroscopy and Imaging (GIPSI) is an experiment designed to address a broad range of topics in high energy astrophysics, and accomplish these goals within a modest payload. The strawman GIPSI described here is scaled to fit within the envelope of a Small Explorer class satellite mission. Even with this small scale, GIPSI is capable of many interesting new scientific discoveries including the detection of <sup>44</sup>Ti in supernovae remnants, polarization in several sources, and solar flare spectra and polarimetry. GIPSI will make high resolution spectral measurements in the energy range from 10–600 keV, and is sensitive to polarization in the energy range from 60–300 keV. GIPSI is nominally a two year mission; in that interval approximately 40 distinct sources will be observed.

GIPSI is designed to combine several key measurement capabilities into one instrument package. Its primary capabilities are good spectral resolution, imaging, and sensitivity to polarization. Spectral resolution is necessary to resolve the break between thermal and non-thermal components in the soft spectra from solar flares, observe narrow line features in supernovae remnants, and cyclotron line features in X-ray binaries. As discussed later, spectral resolution is also valuable in the measurement of polarization. Polarimetry above 60 keV is a relatively

unexplored science with the potential of elucidating the geometry of emission regions in a variety of sources. GIPSI is also an imaging instrument. Imaging is a technique that provides background subtraction, alleviates source confusion, and provides capability to map small regions of the sky.

We present here an instrument sized for a Small Explorer class (SMEX) mission which has sensitivity to achieve the scientific objectives discussed below. GIPSI uses an array of 16 Germanium Strip Detectors (GSDs) located inside a BGO anticoincidence well for background reduction, and a coded-aperture to provide imaging and background subtraction. The spacecraft is 3-axis stabilized and provides GIPSI with all-sky pointing capability, including pointing directly at the sun.

The detectors used in GIPSI are GSDs which combine the excellent energy resolution typical of germanium solid-state detectors with good position resolution. GSDs have advantages in a variety of instrument configurations with very diverse scientific objectives. GIPSI will provide valuable flight experience for GSDs.

## 2 SCIENCE OBJECTIVES

Several scientifically important observations are possible using GIPSI including:

- Study radioactive line emission from galactic supernovae with good angular resolution. Map selected regions of the Galaxy for emission from  $^{44}\text{Ti}$  (68, 78 keV), and  $^{60}\text{Fe}$  (59 keV). These maps will reflect the nucleosynthetic contributions of supernovae, and possibly discover sites of galactic supernovae in  $^{44}\text{Ti}$ . Narrow lines from the decay of radioactive  $^{44}\text{Ti}$  ( $\tau_{1/2} = 46$  yr), are present in supernovae remnants (SNR). A higher energy line (1.157 MeV) has been reported by the COMPTEL instrument on CGRO from Casseopia A<sup>1</sup> at a flux level  $4.2 \pm 0.9 \times 10^{-5} \gamma \text{ cm}^{-2} \text{ s}^{-1}$ . XTE and OSSE place upper limits on the flux at  $\sim 1.5 \times 10^{-5}$ . The sensitivity of GIPSI will detect flux at half the OSSE limits with a  $3\sigma$  sensitivity in a two week observation.
- Detect fresh radioactivity from extragalactic Type Ia supernovae, determine the nature of Type Ia events, and evaluate their use as a cosmic distance indicator.  $^{57}\text{Co}$  lines (122 and 14 keV) from Type II supernovae can be detected to distances of 1.5 Mpc (beyond Andromeda). Late detonation models<sup>2</sup> predict production of  $^{56}\text{Ni}$  sufficient that narrow line flux (158 keV) could be detected out to a distance of 16 Mpc (Virgo) with GIPSI.
- Provide high resolution spectra for several 10's of AGN in the low-energy  $\gamma$ -ray region, study evolution of AGN in this energy band where they exhibit peak luminosity, and support multi-wavelength campaigns of AGN.
- Provide, for the first time, sensitive polarization measurements in hard X-rays in a variety of sources including pulsars, Be-binaries, accretion powered emission from BHCs, AGN, and solar flares. For example:
  - Linear polarization of 19% at 2.6 and 5.2 keV has been detected from the Crab nebula<sup>3</sup> where synchrotron radiation is responsible for a large percentage of the X-ray emission.
  - Cen A has jets of high-velocity matter being ejected from its center. Its gamma-ray spectrum is power law with a strong cut-off above about 1 MeV. The model of Skibo, Dermer, and Kinzer,<sup>4</sup> suggest that the cut-off in the hard X-ray spectrum is a result of a power-law injection spectrum beamed in the direction of the jets in Cen A. The jets are inclined roughly 60 degrees from the line-of-site. Radiation observed at the Earth is Compton scattered in clouds located along the jet. Thus, the scattering geometry of this source is predicted to result in a linear polarization on the order of 60% below 200 keV. Cen A is a relatively bright galaxy, detectable by GIPSI. Polarization measurements would place stringent constraints on the geometry of the emission region.
  - Another good candidate for detecting linear polarization is Cyg X-1, a black hole candidate with strong X-ray emission from the inner regions of an accretion disk around the central object. The hard X-ray emission likely originates from Compton up-scattering of lower energy photons in a thin hot plasma near the central region of the disk. Further, evidence of a reflection component in the X-ray spectrum<sup>5</sup>

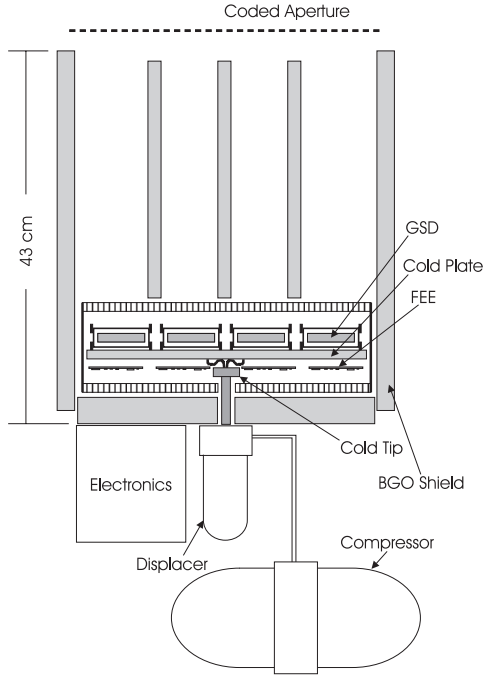


Figure 1: Cross-section schematic diagram of GIPSI showing major instrument subsystems. Detectors are individually housed in hermetic ceramic canisters and mounted on a common cold-plate. The cold plate is in a vacuum cryostat during ground testing. Low-power CMOS Front-End Electronics (FEE) are mounted just below the cold-plate on thermally isolated stand-offs.

suggests that a large percentage of the emission between 10–100 keV is Compton scattered off the accretion disk. Both components of the direct and reflected components of the emission spectrum are likely to be polarized, depending on the geometry of the emission region and the line-of-site of the observer.

- Provide high resolution of cyclotron absorption features in highly magnetized stars such as Her X-1 and 1A 0535+262.
- Study solar flare spectra and electron beaming. A variety of physical processes in solar flares are predicted to produce linearly polarized hard X-rays. The most basic process is Compton reflection of X-rays from a loop off the photosphere itself, which is likely to produce linear polarization on the order of a few percent.<sup>7</sup> Emission above about 50 keV is from a non-thermal population of electrons. Beamed electrons in loops may produce linear polarization on the order of 10%.<sup>8</sup>

### 3 INSTRUMENT

GIPSI is comprised of 16 position sensitive germanium strip detectors. Each GSD has  $5 \times 5 \text{ cm}^2$  active area and is 1 cm thick. The 16 detectors are individually housed in compact, hermetically sealed ceramic canisters. Ceramics are used to minimize feed-through capacitance, thus improving the energy resolution of the detectors. The canisters are mounted on a common cold plate in a vacuum cryostat. Strip electrodes with a 2 mm pitch on opposite faces of the detector collect ionization signal (electrons and holes respectively). Two dimensional positions are determined by the intersection of strips from the opposite faces of the detector with matching signals. Energy resolution typical of a germanium detector ( 2 keV full width half maximum) is achieved, limited by electronics noise. A detailed description of the properties of these detectors is provided by Kroeger *et al.*<sup>9</sup>

There are a total of 800 signals from the germanium detectors. Each will be read out using a low noise CMOS preamplifier and shaping amplifier chip developed for GSDs.<sup>10</sup> The instrument is triggered by a CMOS discriminator and peak-detect circuit on each channel,<sup>11</sup> then digitized with a 12-bit ADC. A signal on any strip

above the lower level discriminator ( $\sim 10$  keV) will cause a trigger. The front end readout is controlled by a Field Programmable Gate Array which ultimately transfers the digitized results to the central computer.

The GSDs and vacuum cryostat are in a BGO well that provides shielding from background radiation, vetos signals from internal radioactivity, and provides coarse collimation of the field of view. The active shield is necessary for celestial observations where the source to background ratio is low. In solar flares, however, the source flux exceeds the background rates and active shielding is not required. Events with a simultaneous energy loss in the GSDs and shield are tagged but not rejected by the on-board logic, so that high rates from solar flares will not paralyze the instrument. Strips in the GSD have an effective area of  $1 \text{ cm}^2$  and are individually analyzed, thus pileup is a concern only for the peak intensity of some X-class flares.

The necessity of annealing the GSDs during flight to compensate for radiation damage over a nominal 2-year period needs further study. However, similar GSDs have been annealed and survived several cycles in the laboratory with no adverse affects. An annealing capability could be added to GIPSI if required.

The front-end computer is a low power 486 CPU which handles zero-suppression and formatting of the data, building histograms, and managing the on-board solid-state storage. Event-by-event data is accumulated with a 12-bit energy resolution, 1 ms time stamp (10-bit), and a 14 bit pixel identifier. These data are stored in a solid-state data recorder along with housekeeping information accumulated at 1 second intervals for downlink. Telemetry contact is made with the spacecraft twice daily. The computer is also in charge of commanding, housekeeping, and other routine, low duty cycle functions. The computer interfaces with the spacecraft computer which provides attitude information and the command interface. Attitude control is precise to 0.5 degree with knowledge to 1 arc minute provided by sun sensors and a low power star sensor.

### 3.1 Efficiency Simulations

The efficiency and usable energy range of the strip detector for polarimetry and imaging have been studied using Monte-Carlo simulations of the GIPSI detector at energies between 80 and 511 keV. Simulations were performed with EGS4,<sup>12</sup> and were modeled with a uniform illumination of a normally incident unpolarized beam. Energy resolution, strip readout (*i.e.* multiple interactions in a strip are summed to one signal), and low level discriminators are all included in the simulation. Figure 2 shows the simulation results for single-pixel, two-pixel, and two-pixel polarimeter events (see polarimeter event selection discussion below). Single-pixel total-energy efficiency starts dropping below the total efficiency above  $\sim 80$  keV, due to the increasing importance Compton scattering and multi-pixel interactions. At higher energies, efficiency decreases due to the decreasing total energy absorption efficiency of the detector and the increasing probability that more than two pixels are involved in an event. The finite size of the interstrip gaps is not included in the Monte-Carlo model. The interstrip gap region is fully active but the ionization signal is divided between the adjacent strips. This effect will decrease the efficiency of *single*-pixel interactions by roughly  $\sim 15\%$  from the simulated results shown in Figure 2. Measurements at 60 keV from a uniform illumination show that 85% of the full energy events are single-pixel, and the remaining 15% share signals between adjacent strips. Fortunately, almost all two-pixel events are useful and do not represent a loss in detector efficiency.

Polarimeter efficiency is calculated as the efficiency of events with two non-adjacent pixels in the Compton-scatter angle range of  $60 < \theta < 120$  degrees. Scatters between adjacent corners are included in the polarimeter efficiency (see below).

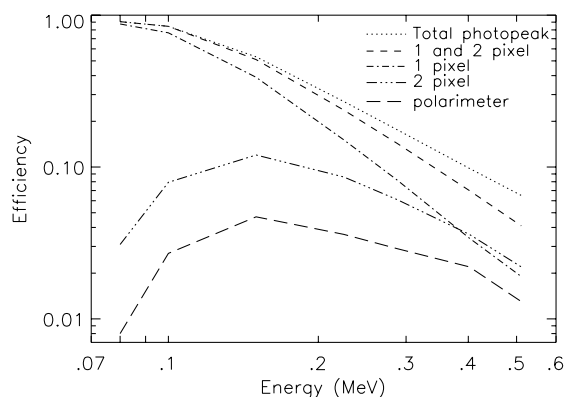


Figure 2: Results of Monte-Carlo simulations. Shown are the efficiencies for single-pixel, dual-pixel, and polarization events. The finite size of the strip gaps is not included in the model.

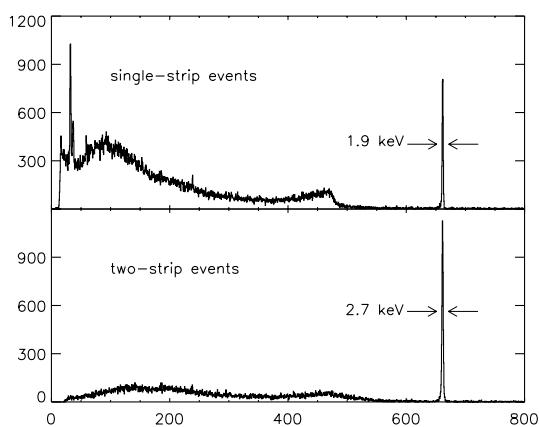


Figure 3: Energy spectra from a uniform illumination of 662 keV gamma-rays from  $^{137}\text{Cs}$ . Shown are the boron-strip spectra for events where energy is deposited in one and two strips of the detector. The FWHM is consistent with the additional electronic noise from readout of multiple strips.

### 3.2 Spectroscopy

Detector performance in terms of energy and position resolution and correction for cross-talk effects has been reported in detail in previous publications<sup>13</sup> and is summarized here. When connected individually, the Full-Width Half-Maximum (FWHM) energy resolution at 60 keV of a single boron strip is 1.4 keV, and 1.7 keV for a single lithium strip. Cross-talk is negligible on the boron-implant face of the detector ( $\sim 0.1\%$ ) and somewhat more significant on the lithium-diffused face ( $\sim 1.5\%$ ) due to the greater thickness of the lithium contacts. It is a simple matter to calibrate and correct for cross-talk between the signals.<sup>9</sup>

Figure 3 shows the boron-strip spectra from a uniform illumination with a  $^{137}\text{Cs}$  source. The first spectrum was obtained by selecting events with signals in only one boron strip. The second spectrum is from events with signals in two boron strips. The signals in each event were summed to produce this histogram. The energy resolution of the total energy peak is consistent with the additional electronic noise from readout of two strips. Similar results are obtained using the lithium strips.

### 3.3 Imaging

Imaging with GIPSI is accomplished using a pin-hole aperture to cast a shadow of the sky onto the GSDs. The aperture pattern is a uniformly redundant array (URA)<sup>14</sup> which has excellent imaging properties over the

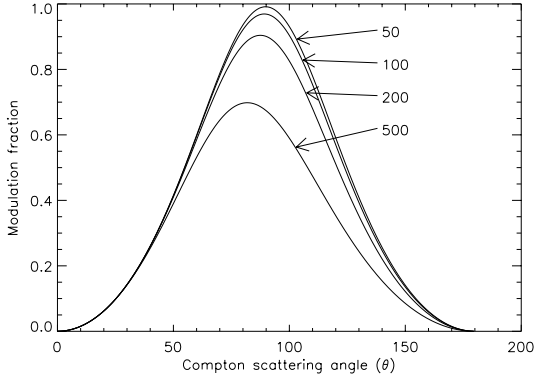


Figure 4: Modulation fraction for a 100% polarized beam, defined as  $A = \frac{d\sigma_{\perp} - d\sigma_{\parallel}}{d\sigma_{\perp} + d\sigma_{\parallel}}$  as a function of Compton scatter angle  $\theta$ . Curves for incident energies of 50, 100, 200, and 500 keV are plotted.

useful field of view. A coarse collimator is used to minimize diffuse-sky background and the effects of sources outside the field of view. The cell size in the aperture is chosen to be 6 mm, thus the GSDs oversample the aperture cells by 3:1, providing optimum “coding power”, *i.e.* maximum sensitivity to point sources anywhere in the field of view.<sup>15</sup>

The distance between the aperture and detector planes is 40 cm. This provides an angular resolution of 0.8 degrees FWHM over a useful field of view of  $\sim 7^{\circ} \times 7^{\circ}$ . Positioning of previously unknown sources will be better than the angular resolution in proportion to the statistical significance of the measurement, limited by the spacecraft aspect accuracy. Angular resolution is adequate to resolve most point sources. The angular resolution will permit measurements of sources with spatial extent on the order of 1-2 degrees.

### 3.4 Polarimetry

Polarization can be measured using Compton-scattering because of the asymmetry in the scattering cross-section relative to the direction of the electric vector of the incident photon (ref) as shown in Figure 4. In the GSD, polarization is measured by observing the direction of scattered gamma rays following a Compton interaction. There are several features of the GSD that are useful for polarimetry measurements below  $\sim 500$  keV:

- High modulation factor: This is achieved, in part, by the good resolution of the scatter azimuth angle  $\phi$  provided by many small pixels, and by selecting events with scatter angles in the range near  $90^{\circ}$  using the measured energy loss and Compton kinematics. The kinematic selection is achievable with the good energy resolution of germanium detectors. The modulation factor we have achieved using GSDs is significantly higher to what is reported for polarimeters using scintillators<sup>16,17</sup> in a similar energy range.
- Greatly improved efficiency as compared to what has been achieved with segmented coaxial germanium or arrays of planar and coaxial germanium.<sup>18,19</sup> The strip detector achieves this higher efficiency because of the finer segmentation, and because any pixel within the detector can be both a scattering and analyzing element.
- The possibility of measuring polarization without rotating the instrument. The strip detector provides full 360 degree coverage of the azimuthal scattering area with small, calibratable anisotropies. A single detector is essentially an array of many small polarimeters; anisotropies due to varying efficiencies of individual elements are averaged out. A non-rotating detector is essential to study time varying sources such as solar flares.
- High rejection of accidental two-pixel events in high-rate measurements such as with solar flares. Accidental coincidences between the scattering and absorbing elements can add significant background to a polarimetry measurement. This background can be reduced by applying kinematic event selection to eliminate events

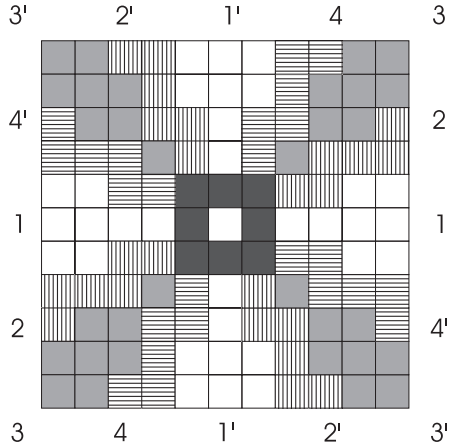


Figure 5: Plot of scatter directions in strip detector and the regions that are used to determine the modulation ratio  $R$ . The horizontal axis is the distance between the two interactions in a direction perpendicular to one set of strips (boron), and the vertical axis is the distance between the other set of strips (lithium). The center of the Figure is for  $\Delta x = 0, \Delta y = 0$ , and corresponds to an event that interacts in exactly one pixel. The dark shaded inner region represents interactions in adjacent pixels which are routinely rejected in standard analysis. The other regions are described in the text.

that are inconsistent with the geometry of the detector and/or inconsistent with a Compton scattering angle near the peak of the scattering cross-section asymmetry curve. In addition, we can disregard coincident events in elements more than a few pixels apart as most likely originating from accidental coincidences.

### 3.4.1 Strip detector polarimeter geometry

Every pixel in the GSD can be both a scattering and analyzing element. The detector is essentially an array of 625 miniature polarimeters (although the efficiency of the edge pixels is lower than the center pixels). Figure 5 shows the geometry of the polarimeter. The central pixel is the scattering element, which is surrounded by a square array of analyzing elements. The array of the analyzing pixels is divided into several regions for binning counts. Selection of the binning regions is somewhat arbitrary. We have selected angular regions that are centered about the symmetry angles of the polarimeter, *i.e.* about the angles of 16 analyzing elements that are separated from the scattering element by one pixel. Because the analyzing elements are arranged in a square (instead of cylindrical) geometry about the central scattering pixel, the scattering efficiency is not identical between the different scattering regions. Region **1** has the highest efficiency, region **3** the lowest. Therefore we cannot simply plot the number of photons scattered into a region versus the mean scattering angle  $\phi$  of that region. Instead we compare the scatter counts between a region **1** – **4** and its complementary (perpendicular) region, indicated as **1'** – **4'** in Figure 5. A region and its complementary region have similar efficiencies, due to the 90 degree rotational symmetry of the detector. There is some anisotropy due to the differing gap sizes between the lithium and boron strips.

We define the measured modulation ratio as,

$$R(\phi) = \frac{N(\phi + 90) - N(\phi)}{N(\phi + 90) + N(\phi)} \quad (1)$$

where  $N(\phi)$  and  $N(\phi + 90)$  are the number of photons scattered in an analyzing region in the direction of  $\phi$ , and the perpendicular direction  $\phi + 90$  respectively. This ratio is maximum in the direction of the incident beam polarization,  $\phi_0$ . This ratio is necessarily smaller than the maximum ratio suggested by Figure 4 for two reasons: the measurements are an average over a range of scatter angles  $\theta$ , and the finite size of the detector elements limits the resolution of the angle  $\phi$ .

A series of event-selection steps are applied to maximize the sensitivity of the GSD polarimeter, and to minimize systematic uncertainties. First, only two-pixel events are retained. Second, two-pixel events between

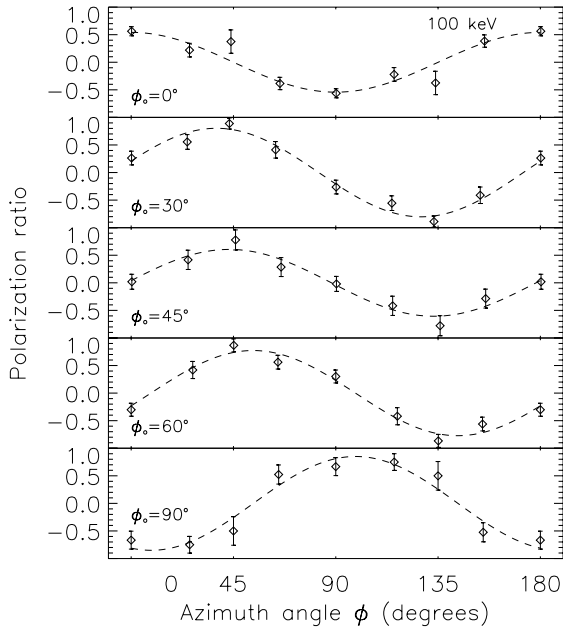


Figure 6: Measured polarization ratio for 100 keV polarized beam as a function of polarization azimuth angle. The beam was oriented with polarization direction  $\phi$  as indicated in each plot.

pixels that share a side are discarded because they are dominated by charge-sharing events where the photon was incident in the region between strips. Scatters between pixels with adjacent corners are treated separately from scatters into regions 1-4. Adjacent-corner scatters have significant interaction efficiency in the GSD, but lower modulation factor because they include scatters over a wider azimuthal angle.

The modulation factor of a polarimeter can be greatly improved by using those Compton scatters which show the greatest asymmetry, *i.e.* with Compton scattering angle near the maximum of the polarization ratio as shown in Figure 4. Based on the energy loss in the analyzing and detecting pixels of the detector, the Compton scatter formula can be used to deduce the Compton scatter angle  $\theta$ . Typically, a range of scatter angles between 60–120 degrees provides good results. This selection is referred as “kinematic” data selection and is only possible in a detector with good energy resolution or a very restrictive geometry. For this data selection to be effective, it is necessary to determine the pixel of the first interaction in order to compute  $\theta$  for each event. Fortunately, below a few 100 keV, the first interaction is usually the smaller energy loss. This becomes a concern for incident energies near 511 keV with the effect of reducing the modulation factor somewhat. One solution for the case when the first pixel is uncertain is to keep an event if the derived scatter angle is in the correct range with the assumption of either pixel being first. The first pixel is generally easy to determine at energies below 300 keV where GIPSI is most sensitive as a polarimeter.

### 3.4.2 Experimental results

Experimental results from polarization measurements at 100 keV are shown in Figure 6. A highly polarized beam was produced by scattering photons from  $^{57}\text{Co}$  (122 keV) by  $90^\circ$  off a scintillator target located a short distance from the strip detector. The resulting polarized beam is normally incident on the strip detector. A photomultiplier detects interactions in the scintillator; readout of the strip detector and scintillator is triggered by a coincidence between the two detectors. Data is stored in an event list for subsequent processing. Separate data sets were acquired with the direction of polarization at several orientations relative to the boron strips of the detector. The beam polarization was oriented at 0, 30, 45, 60 and 90 degrees.

After selection of the total energy absorption events, two-pixel events are sorted from the event list and the kinematic selection applied as described above. The angle  $\phi$  for each binning region is calculated as the average angle of the events scattered into that region. Figure 6 shows the resulting polarimetry ratio for each of the orientations of the polarization vector. For visual effect, the data are plotted over 180 degrees, although only the first four data points are independent. The ratio data are fit to a function  $R = R_0 \cos^2(\phi - \phi_0)$ . For the plots shown in Figure 6 the average value of  $R_0$  is 0.7, whereas the incident beam was 0.97, giving a modulation factor of 0.76. We measured an average modulation factor of  $\sim 0.7$  in a similar experiment with the same GSD using a 290 keV polarized beam.<sup>13</sup>

The GSD polarimeter has some intrinsic anisotropy, thus an unpolarized beam will appear to have a small polarization if the anisotropy is not first measured, then corrected. The chief cause of this anisotropy is probably due to the differences in gaps between the strips on the boron and lithium sides that produce slightly different efficiencies between a given region and its complementary region. In any individual GSD, the magnitude of the anisotropy is equivalent to a polarization of  $<10\%$ . This anisotropy is easily calibrated with an unpolarized beam and corrected. Further, it can be minimized by orienting half of the detectors in GIPSI with lithium strips perpendicular to the other half.

### 3.5 Mission

The preferred orbit for GIPSI is a 500 km circular, low-inclination orbit, thus minimizing exposure to the radiation belts. The orbit decay-time at this altitude should provide a nominal mission in excess of two years. Sensitivity calculations for this orbit are shown in Figures 7 and 8. Sensitivity will be slightly better just after launch and be slightly worse near the end of the two-year mission due to build up of long-lived radioactive spallation products.

Polarization sensitivity of the GSDs (2 mm strip pitch) is maximum from around 80–200 keV, with reasonable sensitivity over a slightly broader range. In a strong source such as the Crab nebula, it should be possible to measure polarization in three or four energy bands. The minimum detectable polarization depends on the intensity the source in the energy band being analyzed. Table 1 provides examples of the minimum detectable polarization by GIPSI for a few selected sources.

Data will be stored on board the spacecraft in a 300 Mbyte solid state data recorder. Telemetry volume is estimated based on an average data rate of 100 events per second, two-pixel interactions in the detectors, and 36 bits per interaction. Housekeeping records will be generated every 1 second and will include spacecraft attitude, clock, and monitor the general health of the instrument. Data from the source field will be telemetered in event-by-event (EBE) mode. Histograms of the energy loss in each detector and shield rates will also be accumulated and stored for transmission. Only housekeeping, rate and histogram data will be stored during periods of Earth occultation. The average daily data volume will be less than 400 Mbit per day which is less than half of the standard downlink capability. Telemetry uplink and downlink will be provided by a single ground station.

GIPSI will develop an observing schedule on a 6-month basis. Typical observations are on the order of 2–6 weeks. GIPSI will also support targets-of-opportunity (ToO) observations in order to observe X-ray transient outbursts (BHC, Be-binaries), solar active regions, and supernovae. Amongst the initial targets for GIPSI observations are Crab nebula/pulsar, Cen A, Cyg X-1, Her X-1, Galactic center region, 3C 273, NGC 4151 (Sy 1.5), IC 4329A (Sy1), NGC 4388 (Sy2). Two or three ToO observations per year are anticipated, possibly triggered by BATSE on CGRO or some other hard X-ray all sky monitor. Examples of transient sources between 1991 and 1994 that probably would have been GIPSI ToOs include: 1A 0535+262, GRS 1008-57, GRS 1915+105, GRO J1655-40, GRO J0422+32, GRO J1719+24, 4U 1543-47, and GRS 1009-49. Other targets that might also be observed in ToO mode include supernovae, 4U 1700-47, Cyg X-1, and others. GIPSI will also support guest investigations and coordinated observation campaigns with other observatories.

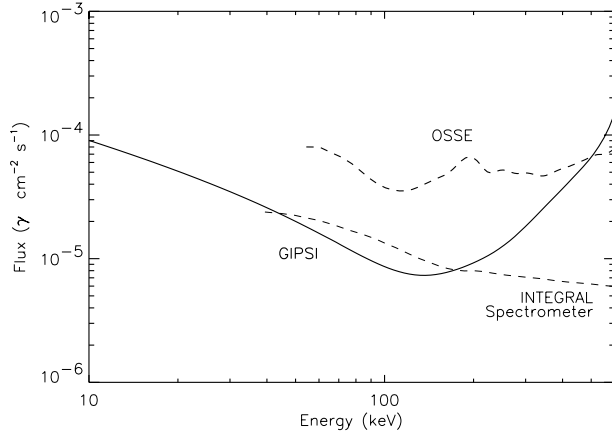


Figure 7: GIPSI sensitivity to narrow lines with a 2 week observation ( $7 \times 10^5$  sec on source). Sensitivities for typical exposures using other instruments are shown for comparison. The OSSE sensitivity curve is for an exposure of  $5 \times 10^5$  sec, and the predicted sensitivity curve for the INTEGRAL Spectrometer is for a  $10^6$  sec exposure.

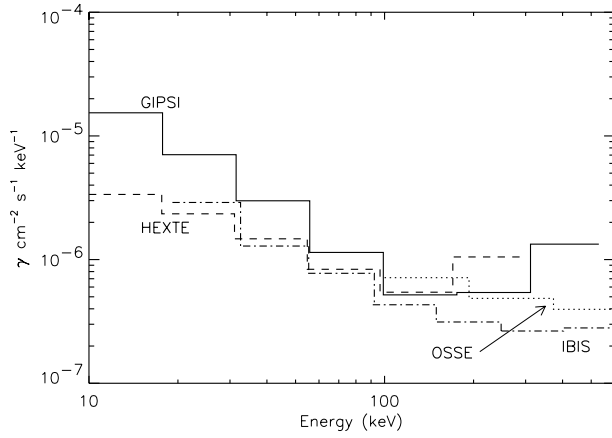


Figure 8: GIPSI sensitivity to continuum emission with 2 week observation of  $7 \times 10^5$  sec on source. The sensitivities of HEXTE, OSSE, and predicted for the INTEGRAL IBIS instrument are plotted for comparison. Typical exposures for these other instruments are  $10^5$ ,  $5 \times 10^5$ , and  $10^6$  sec respectively.

Table 1: Minimum Detectable Polarization ( $3 \sigma$ )

| Source                       | Exposure (weeks) | MDP (%)<br>70–300 keV |
|------------------------------|------------------|-----------------------|
| Crab nebula                  | 2                | 1.4                   |
| Crab pulsar                  | 2                | 5.2                   |
| Cen A                        | 2                | 8.7                   |
| Cyg X-1                      | 2                | 1.6                   |
| 1A0535+262                   | 2                | 2.9                   |
| GRO J1655-40                 | 2                | 3.5                   |
| NGC 4151                     | 6                | 14.1                  |
| 3C 273                       | 6                | 16.0                  |
| July 1, 1980 flare<br>(X2.5) | 200 sec          | 5.3                   |

Table 2: WEIGHT and POWER

|                           | Mass (kg)  | Power (W)  |
|---------------------------|------------|------------|
| Detectors (16 GSDs)       | 5          |            |
| Detector electronics      | 5          | 8          |
| Cold plates/cryostat      | 10         |            |
| Cryocooler                | 11         | 45         |
| Shield/BGO                | 140        |            |
| Shield PMTs               | 4          | 5          |
| Shield electronics        | 5          | 2          |
| Coded aperture            | 6          |            |
| Central electronics       | 5          | 17         |
| Heaters/MLI               | 2          | 3          |
| Mechanical support/frame  | 18         |            |
| Cables                    | 5          |            |
| Attachments               | 8          |            |
| SMEX Lite Protoflight S/C | 75         | 75         |
| <b>TOTAL</b>              | <b>299</b> | <b>155</b> |

## 4 CONCLUSIONS

The GIPSI experiment provides sensitivity to study many of the important sources in high-energy astrophysics. It is capable of detecting and mapping the  $^{44}\text{Ti}$  lines resulting from recent galactic supernovae, observations of soft spectra and cyclotron features such as those from 1A0535+249 and Her X-1. GIPSI will also contribute new information on the polarization of hard X-rays from a variety of different sources. Polarization will provide for the first time direct information on the geometry of the emission region. Polarization is expected from AGN, solar flares, the Crab pulsar, and from transient X-ray novae and low mass X-ray binaries. The polarimetry capabilities of GIPSI are not possible with those instruments currently being planned for gamma-ray astronomy. GIPSI represents a significant advance in this field.

Several new technologies go into the GIPSI instrument. These include GSDs, ceramic detector packaging, and custom CMOS electronics. The unique capabilities of GSDs in GIPSI, such as provided by the fine segmentation, will generate interesting technical data on internal radioactivity in germanium detectors and surrounding materials, important for the design and construction of a major mission using similar detectors. The technical advances developed for GIPSI are necessary steps for the next generation of instruments using GSDs.

We have demonstrated that the GSD is useful as a gamma-ray polarimeter with very high modulation factors and low systematic polarization bias. Further, it is not necessary to rotate the GSD polarimeter to modulate the polarized signal, thus a GSD polarimeter is simple to construct and is not affected by time-variable sources. Additional studies of the GSD as a polarimeter are planned to push the sensitivity as high as possible and to study small systematic effects that need to be calibrated. Plans include measurements at additional energies covering the energy range of scientific interest and with longer exposures to push the minimum detectable polarization level to  $\sim 1\%$ .

## 5 REFERENCES

1. Schönfelder, V. *et al.*, 1996, 3<sup>rd</sup> Compton Science Symposium, München, Germany 1995.
2. Yamaoka, H., *et al.*, "Late Detonation Models for the Type Ia Supernovae SN 1991T and SN 1990N", 1992, ApJ, 393, L55.
3. Weisskopf, M.C., *et al.* "A Precision Measurement of the X-ray Polarization of the Crab Nebula Without Pulsar Contamination", 1978, ApJ, 220, L117.
4. Skibo, J.G., Dermer, C.D., and Kinzer, R.L., "Is the High-Energy Emission from Centaurus A Compton-Scattered Jet Radiation?", 1994, ApJ, 426, L23.
5. Done, C., *et al.*, "An Ionized Accretion Disk in Cygnus X-1", 1992, ApJ, 395, 275.
6. Johnson W.N., *et al.*, 1995, "Advanced Telescope for High Energy Nuclear Astrophysics (*ATHENA*)", SPIE Vol. 2518, ed. O.H.W. Siegmund & J.V. Vallagra, 74.
7. Henoux, J.C., "Anisotropy and Polarization of Solar X-ray Bursts", 1975, Solar Phys., 42, 219.
8. Leach, J., Emslie, A.G., and Petrosian, V. 1985, Solar Phys., 96, 311.
9. Kroeger, R.A., *et al.*, 1995, "Spatial Resolution and Imaging of Gamma-Rays with Germanium Strip Detectors", SPIE Vol. 2518, ed. O.H.W. Siegmund & J.V. Vallagra, 236.
10. Kroeger, R.A., *et al.*, "Charge Sensitive Preamplifier and Pulse Shaper using CMOS process for Germanium Spectroscopy Detector", IEEE Trans. Nucl. Sci, Vol 42, No 4, 921.
11. Ericson, M.N., *et al.*, "A Low-Power, CMOS Peak Detect and Hold Circuit for Nuclear Pulse Spectroscopy", IEEE Trans. Nucl. Sci, Vol 42, No 4, 724.
12. Nelson, W.R., Hirayama, H., and Rogers, D., 1985, SLAC report 265.

13. Inderhees, S.E., *et al.*, 1996, "Spectroscopy, Imaging and Compton-scatter Polarimetry with a Germanium Strip Detector", IEEE Trans. Nucl. Sci., Vol 43, No. 3, 1467.
14. Fenimore E.E., and Cannon T.M., "Coded aperture imaging with uniformly redundant arrays", 1978, Applied Optics, 17, 337.
15. Skinner, G.K., "Coding (and decoding) coded mask telescopes", 1995, L. Bassani and G. Di Cocco, (eds.), *Imaging in High Energy Astronomy*, Kluwer Academic Publishers.
16. Tomita, H. *et al.*, "Basic Performance of Unitized Compton Scattering Type Polarimeter", IEEE Trans. Nucl. Sci, Vol 43, No 3, 1527.
17. Costa, E., *et al.*, " Design of a Scattering Polarimeter for Hard X-ray Astronomy", 1995, NIM A.
18. Sareen, R.A., *et al.*, "High-resolution integrated germanium Compton polarimeter for the  $\gamma$ -ray energy range 80 keV - 1 MeV", 1995, Rev. Sci. Instrum. 66 (6), 3653.
19. von der Werth, A., *et al.*, "Two Compton polarimeter constructions for modern standard  $\gamma$ - spectroscopy", 1995, Nucl. Instrum. and Methods A 357, 458.